Letter | Editors' Suggestion

Probing the topology of the quantum analog of a classical skyrmion

O. M. Sotnikov,[1] V. V. Mazurenko,[1,*] J. Colbois,[2] F. Mila,[2] M. I. Katsnelson,[3,1] and E. A. Stepanov[4,1]

[1]*Theoretical Physics and Applied Mathematics Department, Ural Federal University, Mira Street 19, 620002 Ekaterinburg, Russia*

[2]*Institute of Physics, École Polytechnique Fédérale de Lausanne (EPFL), CH-1015 Lausanne, Switzerland*

[3]*Institute for Molecules and Materials, Radboud University, Heyendaalseweg 135, 6525 AJ, Nijmegen, Netherlands*

[4]*I. Institute of Theoretical Physics, University of Hamburg, Jungiusstrasse 9, D-20355 Hamburg, Germany*

(Received 4 July 2020; revised 18 November 2020; accepted 21 January 2021; published 12 February 2021)

In magnetism, skyrmions correspond to classical three-dimensional spin textures characterized by a topological invariant that keeps track of the winding of the magnetization in real space, a property that cannot be easily generalized to the quantum case since the orientation of a quantum spin is, in general, ill defined. Moreover, as we show, the quantum skyrmion state cannot be directly observed in modern experiments that probe the local magnetization of the system. However, we show that this novel quantum state can still be identified and fully characterized by a special local three-spin correlation function defined on neighboring lattice sites—the scalar chirality—which reduces to the classical topological invariant for large systems and which is shown to be nearly constant in the quantum skyrmion phase.

DOI: 10.1103/PhysRevB.103.L060404

The broad use of topological language is one of the main trends in contemporary physics, including condensed-matter physics and even materials science [1–11]. Numerous nontrivial topological effects in superfluid helium-3 [4], the concept of topological quantum phases in strongly correlated systems [5,6], topologically protected zero-energy states in magnetic field and other topology-related issues in graphene [7], and the quickly growing field of topological insulators [9] provide excellent examples. When considering quantum systems, we usually deal with topology in reciprocal k space [5,6], whereas for classical systems topological protection of defects of a different kind [8] plays a crucial role.

Among such defects, magnetic skyrmions [12] are currently attracting special attention due to perspectives to use them in magnetic information storage [13–15]. The progress in the development of experimental techniques [16–23] poses new challenges for the theory and numerical simulations of nanoscale topological structures [24]. Thus, skyrmions with the characteristic size of a few nanometers have already been observed experimentally [25,26] and predicted theoretically in frustrated magnets [27–29], narrow-band Mott insulators under high-frequency light irradiation [30], and Heisenberg-exchange-free systems [31]. On such small characteristic length scales compared to the lattice constant, quantum effects cannot be neglected. The same difficulty also arises in low-dimensional systems with small spin (e.g., $S = 1/2$) [32–35] and itinerant systems with delocalized magnetic moments.

It is, however, not at all clear what a quantum skyrmion (that is, a skyrmion in a system of quantum spins) could be. There is, indeed, no way to introduce a topological charge for the *quantum* spin case which would protect quantum skyrmions similar to the topological protection in classical systems [8]. Physically, this fact means that topologically protected classical spin configurations are, generally speaking, not robust with respect to quantum tunneling, which can transform them into topologically trivial states. Nevertheless, one can assume that the existence of topologically protected *classical* magnetic configurations should influence, in some way, the properties of the corresponding quantum systems.

This fundamental problem was not clarified in the previous attempts to introduce "quantum skyrmions." Instead, description of this quantum state was done either semiclassically assuming that the magnetization dynamics is dominated by classical magnetic excitations that emerge on top of the symmetry-broken ground state of the system [36–38] or by means of the Holstein-Primakoff transformation, which allows one to compute only quantum corrections to the classical solution [39]. Also, the standard identification of a skyrmion by its magnetization pattern was used in recent works [40,41] in which topological states of small clusters embedded in a ferromagnetic environment were investigated. However, this does not take into account the fact that, strictly speaking, the corresponding states are not actually "topological" in the sense of some rigorous protection. This problem will be addressed in this work.

Characterization of a quantum skyrmion. Conceptually, the quantum skyrmion problem is somewhat similar to the formation of the antiferromagnetic ordering in quantum systems [42]. Whereas the classical skyrmion solution on the lattice is characterized by a distinct magnetic pattern, in the infinite quantum system all lattice sites are identical and have the same value of the local magnetization. Assuming that modern Lorentz and spin-polarized scanning tunneling microscopy (SPSTM) techniques weakly affect the quantum system, the measurement of the quantum skyrmion state will thus result in the same value of the local magnetization for all lattice sites (see Fig. 1, right). In the case of antiferromagnets [42], the appearance of sublattices is expected to be induced by applying a staggered field that selects the classical Néel state

*vmazurenko2011@gmail.com

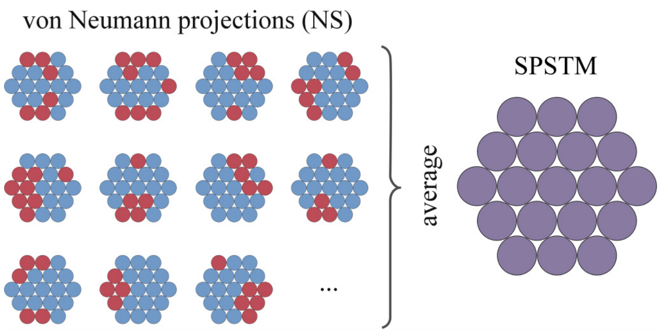

FIG. 1. Schematic representation of the local magnetization measurements of the quantum skyrmion state realized on a 19-site cluster. Upon individual von Neumann measurements, this state collapses to different basis functions shown in the left panel. The average of the local magnetization over all basis functions results in a uniform magnetization pattern that could be observed in the SPSTM experiment (right panel).

from the quantum solution of the problem, but contrary to the case of ferromagnets, this field is not very physical, and it is not easy at all to understand how it can be realized in practice. However, the same can be achieved with the use of the analog of the quantum Zeno effect [43,44], that is, by performing repeated local (von Neumann) measurements of the spin [45–47], which can possibly be realized in inelastic x-ray or neutron scattering experiments. This strong influence on the quantum system will result in the collapse of the wave function to one of the possible basis states with a certain probability via formation of the "decoherence waves" [46].

For the quantum skyrmion case, it turns out that these states do not resemble the classical skyrmion solution. To demonstrate this point, we consider a particular example, the quantum skyrmion state discussed below (2) stabilized on a 19-site cluster with periodic boundary conditions at magnetic field $B = 0.4$. Von Neumann measurements of the local magnetization are modeled using a quantum computer simulator as implemented in the QISKIT package [48]. To this aim we obtain the ground state of the considered system and use it for initialization of qubits. After that, each qubit is measured several times to get the different basis functions demonstrated in the left panel of Fig. 1. Since the considered quantum system is translationally invariant, the local magnetization of the ground state averaged over all basis functions $\langle \hat{S}_i^z \rangle = \langle \Psi_0 | \hat{S}_i^z | \Psi_0 \rangle$ is uniform. Therefore, contrary to the classical skyrmion case, the quantum skyrmion state cannot be detected in any modern experiment that performs a simple local measurement of the magnetization.

Instead, one could calculate the momentum-space representation of the more complicated spin-spin correlation function (structure factor), and if there is magnetic ordering, it is signaled by the development of Bragg peaks at momenta that correspond to the wave vectors **q** of the ordering, as in antiferromagnets. Since the classical skyrmion can be considered as a superposition of spin spirals, a similar pattern of Bragg peaks is expected for a quantum skyrmion state. However, due to the quantum nature of the problem and in contrast to the classical case, the quantum helical phase is also characterized by the quantum superposition of spin spirals. Therefore, as we demonstrate below, the structure factor also does not allow us to distinguish between these two phases of the quantum system.

Strictly speaking, even in the classical case the spin-spin correlation function is also not a sufficient measure for a skyrmion state because different skyrmion, vortex, bubble, and multidomain phases are indistinguishable on the level of the structure factor (see, e.g., [49,50]), and some more complicated correlation functions should be used as discussed in the Supplemental Material (SM) [51]. The classical skyrmion state is actually characterized by a topological invariant which, for continuum models of magnetism, is given by the following expression:

$$Q = \frac{1}{4\pi} \int \mathbf{m} \cdot [\partial_x \mathbf{m} \times \partial_y \mathbf{m}] dx\, dy, \tag{1}$$

which counts the number of times the magnetization $\mathbf{m}(r)$ wraps around a sphere. This characterization depends in an essential way on the relative orientation of the local spins, information which cannot be extracted from the quantum ground state for the reasons explained above.

The fundamental problem is thus how to generalize the classical topological invariant (1) to the quantum case. On a lattice, the proper version of the classical topological invariant was proposed by Berg and Lüscher [52]. According to their idea, the winding of the magnetization can be approximated by a sum of all spherical surfaces that are formed by three neighboring spins. Unfortunately, as shown in the SM [51], their expression for the skyrmion number Q_{BL} cannot be easily converted into a linear quantum operator. What we propose here is to use a discrete version of the topological invariant, the scalar chirality (see below). As we shall see, this quantity, which is naturally defined for both classical and quantum spins, captures the noncollinearity of neighboring spins, and it turns out to be almost constant inside skyrmion phases for both classical and quantum spins. In the quantum case, the scalar chirality reduces to a local quantity defined for nearest-neighbor spin operators, leading to a general and flexible characterization of skyrmions.

Results. We start with the following lattice Hamiltonian of a quantum spin model:

$$\hat{H} = \sum_{ij} J_{ij} \hat{\mathbf{S}}_i \cdot \hat{\mathbf{S}}_j + \sum_{ij} \mathbf{D}_{ij} [\hat{\mathbf{S}}_i \times \hat{\mathbf{S}}_j] + \sum_i B^z \hat{S}_i^z. \tag{2}$$

Here, J_{ij} is the isotropic Heisenberg exchange interaction. $\mathbf{D}_{ij}$ is an in-plane vector that points in the direction perpendicular to the bond between neighboring i and j sites and describes the Dzyaloshinskii-Moriya interaction (DMI). **B** is an external uniform magnetic field applied along the z direction. Quite generally, the competition between the exchange interaction and the DMI leads to the formation of a classical skyrmion that is usually stabilized by a nonzero magnetic field.

Let us look at the phase diagram of the model of Eq. (2) on the triangular lattice. To compare the classical and quantum spin-1/2 cases, we have chosen to work on a 19-site cluster that is one of the largest systems for which the exact diagonalization solution can be obtained [53]. The exchange interaction is set to $J = -0.5D$, where D is the length of the DMI vectors, to produce a nanoskyrmion compatible with

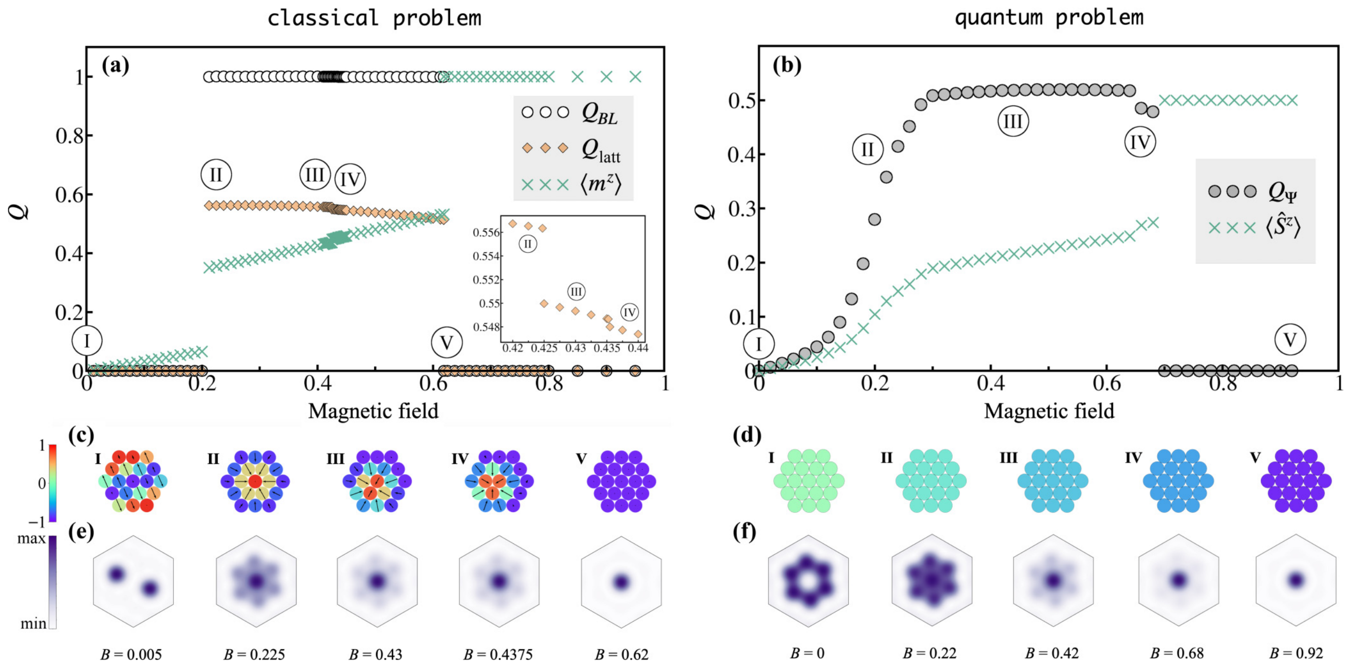

FIG. 2. Complete set of observables describing skyrmions in the classical and quantum cases. (a) and (b) Skyrmion number and average magnetization, (c) and (d) local magnetization pattern of the lattice, and (e) and (f) structure factors as a function of magnetic field for the classical (left panels) and quantum (right panels) problems for a 19-site triangular lattice with periodic boundary conditions. Roman numbers denote different phases. Since the classical ground state is many-fold degenerate we have chosen a representative pattern for the magnetization panel in (c). The inset in (a) shows three different types of classical skyrmions revealed in the intermediate phase by the scalar chirality.

this cluster size. The main results are summarized in Fig. 2. The classical model has been solved for unit magnetization vectors. After that classical energies calculated for different magnetic fields have been normalized to compare the result with the quantum solution.

For the classical case, the presence of three main phases is already clear from the average magnetization $\langle m^z \rangle$ [Fig. 2(a)], which exhibits two jumps at $B_{c1} \simeq 0.21$ and $B_{c2} \simeq 0.6$, indicating strongly first order phase transitions and major reorientations of the spins. However, a closer look at the real-space orientation of the spins [Fig. 2(c)] shows that in the low-field phase the spins are coplanar (I), while in the intermediate phase the spins form three different 3d textures (II, III, and IV) in spin space, which are hardly distinguishable from the energy plot (see the SM [51]). Above $B_{c2} \simeq 0.6$, the spins are fully polarized (V), so B_{c2} is the saturation field. To further identify the nature of the various phases, it is useful to look at several additional properties. The first one is the static longitudinal spin structure factor defined as $X^{\parallel}_{\mathbf{q}} = \langle \hat{S}^z_{\mathbf{q}} \hat{S}^z_{-\mathbf{q}} \rangle$. Figure 2(e) shows that in the low-field phase, it exhibits two Bragg peaks at opposite wave vectors $\mathbf{q}$ and $-\mathbf{q}$, typical of a helical state of pitch vector $\mathbf{q}$. In the intermediate phase, the structure factor is less specific. It looks like the superposition of three pairs of Bragg peaks rotated by $\pi/3$ and of a Bragg peak at the zone center. This is, of course, consistent with a skyrmion structure that, together with the superposition of enclosed spin spirals, is associated with the ferromagnetic ordering along the skyrmion boundary. However, as we have pointed out above, the real identification comes from the topological invariant Q_{BL}, which is calculated here using the Berg-Lüscher approach [52]. As expected, we observe that this invariant is equal to unity in the intermediate phase and vanishes outside it [Fig. 2(a)]. Importantly, neither the structure factor nor the topological invariant can reflect the presence of three types of skyrmions in the intermediate phase.

Let us now try to perform an analysis similar to that for the quantum case. From the average magnetization [Fig. 2(b)], three regimes emerge, but compared to the classical case, the first transition is rounded. Indeed, $\langle \hat{S}^z \rangle$ shows a rapid but smooth increase at a field $B_{\Psi 1} \simeq 0.3$ and a jump at $B_{\Psi 2} \simeq 0.7$. The identification of the nature of these phases is, by far, not as simple, however. First of all, as anticipated in the introduction, the expectation value of the local spin is uniform. So it is impossible to detect a planar or 3d texture from this observable, as can be seen from Fig. 2(d). The natural idea is then to turn to the structure factor [Fig. 2(f)]. However, there is no qualitative difference between low and intermediate fields: in both cases, there are six maxima forming a hexagon and a maximum at the zone center, as in the skyrmion phase of the classical case.

Does this result mean that there is a single phase between zero field and saturation and no well-defined skyrmion phase? Not necessarily. Indeed, if we think in semiclassical terms, the effect of quantum fluctuations on a helical phase will be to stabilize a linear combination of helices if there are different choices of equivalent wave vectors, and indeed, here there are three equivalent choices of pitch vector. So if the low-field phase is the quantum version of the helical phase, we indeed expect to have a hexagon of peaks. The problem is that this is also expected in the case of a skyrmion phase. So it is possible that there are two different phases for quantum spins as well. It is just impossible to distinguish them with the structure factor.

This example clearly calls for an alternative characterization of quantum skyrmions. The solution we propose is based on the following remarks. First of all, the fundamental difference between a classical helical state and a classical skyrmion is that the helical state is a coplanar structure (all spins lie in a given plane), while a skyrmion is a 3*d* texture. So these structures can be distinguished by the mixed product of three spins, $\mathbf{S}_i \cdot [\mathbf{S}_j \times \mathbf{S}_k]$, where i, j, and k are three arbitrary lattice sites. Indeed, this expression will be exactly zero for a helical state but not for a skyrmion. In fact, the skyrmion invariant involves a similar mixed product of three magnetization vectors because the discrete form of the classical topological invariant (1) can be written as [54]

$$Q_{\text{latt}} = \frac{1}{8\pi} \sum_{\langle ijk \rangle} \mathbf{m}_i \cdot [\mathbf{m}_j \times \mathbf{m}_k]. \tag{3}$$

Here $\mathbf{m}_i$, $\mathbf{m}_j$, and $\mathbf{m}_k$ are classical magnetization vectors of length 1, and the summation runs over all nonequivalent elementary triangles that connect neighboring i, j, and k sites. This quantity is known in other contexts as the *scalar chirality*, a term we will use from now on.

Importantly, as we show in the SM [51], the scalar chirality (3) coincides with the topological invariant (1) in the classical limit of the skyrmion when the magnetization slowly varies with respect to the lattice constant. For nanoskyrmions, whose typical length scale is comparable to the lattice constant, a more precise result for the topological invariant is given by the Berg-Lüscher approximation. Still, the scalar chirality is equally good when it comes to distinguishing a helical phase from a skyrmion phase. Indeed, it vanishes identically in a helical phase because it is strictly coplanar, and it does not do so for a 3*d* texture. For the classical case this fact is illustrated in Fig. 2(a). A closer look at the scalar chirality in the intermediate range of magnetic fields presented in the inset allows one to distinguish three skyrmion phases. They are characterized by the different sizes and structures of the magnetic pattern, which are illustrated in Fig. 2(c) in panels II, III, and IV. Thus, contrary to the topological number Q_{BL}, the scalar chirality is sensitive to different types of magnetic skyrmions.

Now, the main advantage of the scalar chirality over the Berg-Lüscher invariant when it comes to quantum systems is that this quantity can be interpreted as a linear operator for quantum spins, so that a ground state indicator can be defined by simply calculating the expectation value of this operator in the ground state. This leads to the following simple definition of the quantum scalar chirality:

$$Q_\Psi = \frac{N}{\pi} \langle \hat{\mathbf{S}}_1 \cdot [\hat{\mathbf{S}}_2 \times \hat{\mathbf{S}}_3] \rangle, \tag{4}$$

where N is the number of nonoverlapping elementary triangular plaquettes that cover the lattice. Labels 1, 2, and 3 depict three different spins that form an elementary plaquette. Here we used the fact that the quantum ground state of the system is translationally invariant, so that the value of the scalar chirality is the same for any elementary triangle. Therefore, the local three-spin correlation function defined on neighboring lattice sites (4) already gives complete information about the topology of the entire quantum system, something that is impossible in the classical case.

As shown in Fig. 2(b), Q_Ψ behaves differently in low-, intermediate-, and high-field phases. Contrary to the classical case, at low fields ($B_{\Psi 1} < 0.3$) the quantum chirality increases gradually with the magnetization. Approaching the intermediate regime, Q_Ψ saturates and remains nearly constant in a very broad range of magnetic fields. This remarkable result cannot be simply interpreted as a freezing of the system since the magnetization keeps growing as in the low-field phase, implying that the quantum ground state of the system evolves continuously. Finally, at the critical field $B_{\Psi 2} \simeq 0.7$, the system enters the fully polarized regime, as indicated by the stepwise decrease of the quantum chirality to zero. The physical picture for the low-field phase is that the ground state is coplanar at zero magnetic field. But instead of remaining coplanar as in the classical case, the linear combination of helical states in the quantum system acquires a noncoplanar structure upon increasing the field. In this case, spins progressively move out of the plane in the direction of the field, which results in a nonzero value of the scalar chirality proportional to the tilting angle. By contrast, in the intermediate phase, the relative angle between spins does not change. It is the collective orientation of the skyrmion spin texture that allows the system to continue developing magnetization.

Conclusion. We have introduced and analyzed a quantum state of a spin system—a quantum skyrmion. We have shown that this state can be fully characterized only by the expectation value of a skyrmion operator related to the local quantum scalar chirality of three neighboring spins. Indeed, in close analogy to the topological invariant that keeps track of the winding in classical skyrmions, the expectation value of the skyrmion operator is field independent to very high accuracy inside the skyrmion phase, in contrast to the simple superposition of spin orderings, where it changes a lot with the field. The value at which it stabilizes is related to the size of the skyrmion, and it would approach unity for very large skyrmions. This reduction factor is related to the value of the nearest-neighbor correlation function and can be independently estimated, so that, if necessary, the expectation value of the skyrmion operator could also be used to estimate the number of skyrmions in a quantum nanoskyrmion structure. We believe that our results can stimulate the development of experimental techniques to locally probe the topology of the entire quantum system. For instance, the impact of the scalar chirality can be seen in the topological Hall effect [17,55–57], in the finite topological orbital moment [58–63], and in nonlinear optical experiments [64–67].

Acknowledgments. We thank S. Brener for interesting discussions. The work of V.V.M., O.M.S., and E.A.S. was supported by Russian Science Foundation Grant No. 18-12-00185. The work of J.C. and F.M. is supported by the Swiss National Science Foundation. The work of M.I.K. is supported by the European Research Council via Synergy Grant No. 854843 - FASTCORR.

[1] *Geometric Phases in Physics*, edited by A. Schapere and F. Wilczek (World Scientific, Singapore, 1989).

[2] D. J. Thouless, *Topological Quantum Numbers in Nonrelativistic Physics* (World Scientific, Singapore, 1998).

[3] M. Nakahara, *Geometry, Topology, and Physics*, 2nd ed. (Taylor and Francis, London, 2003).

[4] G. E. Volovik, *The Universe in a Helium Droplet* (Clarendon, Oxford, 2003).

[5] X.-G. Wen, *Quantum Field Theory of Many-Body Systems* (Oxford University Press, Oxford, 2004).

[6] B. Zeng, X. Chen, D.-L. Zhou, and X.-G. Wen, *Quantum Information Meets Quantum Matter* (Springer, Berlin, 2019).

[7] M. I. Katsnelson, *The Physics of Graphene*, 2nd ed. (Cambridge University Press, Cambridge, 2020).

[8] N. D. Mermin, The topological theory of defects in ordered media, Rev. Mod. Phys. **51**, 591 (1979).

[9] X.-L. Qi and S.-C. Zhang, Topological insulators and superconductors, Rev. Mod. Phys. **83**, 1057 (2011).

[10] F. D. M. Haldane, Nobel Lecture: Topological quantum matter, Rev. Mod. Phys. **89**, 040502 (2017).

[11] J. M. Kosterlitz, Nobel Lecture: Topological defects and phase transitions, Rev. Mod. Phys. **89**, 040501 (2017).

[12] A. N. Bogdanov and D. A. Yablonskii, Thermodynamically stable 'vortices' in magnetically ordered crystals. The mixed state of magnets, ZhETF **95**, 178 (1989) [Sov. Phys. JETP **68**, 101 (1989)].

[13] F. Jonietz, S. Mühlbauer, C. Pfleiderer, A. Neubauer, W. Münzer, A. Bauer, T. Adams, R. Georgii, P. Böni, R. A. Duine, K. Everschor, M. Garst, and A. Rosch, Spin transfer torques in MnSi at ultralow current densities, Science **330**, 1648 (2010).

[14] A. Fert, V. Cros, and J. Sampaio, Skyrmions on the track, Nat. Nanotechnol. **8**, 152 (2013).

[15] R. Tomasello, E. Martinez, R. Zivieri, L. Torres, M. Carpentieri, and G. Finocchio, A strategy for the design of skyrmion racetrack memories, Sci. Rep. **4**, 6784 (2014).

[16] S. Mühlbauer, B. Binz, F. Jonietz, C. Pfleiderer, A. Rosch, A. Neubauer, R. Georgii, and P. Böni, Skyrmion lattice in a chiral magnet, Science **323**, 915 (2009).

[17] A. Neubauer, C. Pfleiderer, B. Binz, A. Rosch, R. Ritz, P. G. Niklowitz, and P. Böni, Topological Hall Effect in the *A* Phase of MnSi, Phys. Rev. Lett. **102**, 186602 (2009).

[18] W. Münzer, A. Neubauer, T. Adams, S. Mühlbauer, C. Franz, F. Jonietz, R. Georgii, P. Böni, B. Pedersen, M. Schmidt, A. Rosch, and C. Pfleiderer, Skyrmion lattice in the doped semiconductor $Fe_{1-x}Co_xSi$, Phys. Rev. B **81**, 041203(R) (2010).

[19] X. Z. Yu, Y. Onose, N. Kanazawa, J. H. Park, J. H. Han, Y. Matsui, N. Nagaosa, and Y. Tokura, Real-space observation of a two-dimensional skyrmion crystal, Nature (London) **465**, 901 (2010).

[20] N. Nagaosa and Y. Tokura, Topological properties and dynamics of magnetic skyrmions, Nat. Nanotechnol. **8**, 899 (2013).

[21] O. Janson, I. Rousochatzakis, A. A. Tsirlin, M. Belesi, A. A. Leonov, U. K. Rößler, J. van den Brink, and H. Rosner, The quantum nature of skyrmions and half-skyrmions in Cu_2OSeO_3, Nat. Commun. **5**, 5376 (2014).

[22] W. Li *et al.*, Anatomy of skyrmionic textures in magnetic multilayers, Adv. Mater. **31**, 1807683 (2019).

[23] S. Zhang, G. van der Laan, J. Müller, L. Heinen, M. Garst, A. Bauer, H. Berger, Ch. Pfleiderer, and T. Hesjedal, Reciprocal space tomography of 3D skyrmion lattice order in a chiral magnet, Proc. Natl. Acad. Sci. USA **115**, 6386 (2018).

[24] C. H. Back, V. Cros, H. Ebert, K. Everschor-Sitte, A. Fert, M. Garst, T. Ma, S. Mankovsky, T. Monchesky, M. V. Mostovoy, N. Nagaosa, S. Parkin, C. Pfleiderer, N. Reyren, A. Rosch, Y. Taguchi, Y. Tokura, K. von Bergmann, and J. Zang, The 2020 skyrmionics roadmap, J. Phys. D **53**, 363001 (2020).

[25] S. Heinze, K. von Bergmann, M. Menzel, J. Brede, A. Kubetzka, R. Wiesendanger, G. Bihlmayer, and S. Blügel, Spontaneous atomic-scale magnetic skyrmion lattice in two dimensions, Nat. Phys. **7**, 713 (2011).

[26] N. Romming, C. Hanneken, M. Menzel, J. E. Bickel, B. Wolter, K. von Bergmann, A. Kubetzka, and R. Wiesendanger, Writing and deleting single magnetic skyrmions, Science **341**, 636 (2013).

[27] T. Okubo, S. Chung, and H. Kawamura, Multiple-q States and the Skyrmion Lattice of the Triangular-Lattice Heisenberg Antiferromagnet under Magnetic Fields, Phys. Rev. Lett. **108**, 017206 (2012).

[28] A. O. Leonov and M. Mostovoy, Multiply periodic states and isolated skyrmions in an anisotropic frustrated magnet, Nat. Commun. **6**, 8275 (2015).

[29] S.-Z. Lin and S. Hayami, Ginzburg-Landau theory for skyrmions in inversion-symmetric magnets with competing interactions, Phys. Rev. B **93**, 064430 (2016).

[30] E. A. Stepanov, C. Dutreix, and M. I. Katsnelson, Dynamical and Reversible Control of Topological Spin Textures, Phys. Rev. Lett. **118**, 157201 (2017).

[31] E. A. Stepanov, S. A. Nikolaev, C. Dutreix, M. I. Katsnelson, and V. V. Mazurenko, Heisenberg-exchange-free nanoskyrmion mosaic, J. Phys.: Condens. Matter **31**, 17LT01 (2019).

[32] J. Schliemann and F. G. Mertens, Vortices in quantum spin systems, Eur. Phys. J. B **9**, 237 (1999).

[33] M. Troyer and U.-J. Wiese, Computational Complexity and Fundamental Limitations to Fermionic Quantum Monte Carlo Simulations, Phys. Rev. Lett. **94**, 170201 (2005).

[34] A. M. Läuchli, J. Sudan, and E. S. Sørensen, Ground-state energy and spin gap of spin-$\frac{1}{2}$ kagomé-Heisenberg antiferromagnetic clusters: Large-scale exact diagonalization results, Phys. Rev. B **83**, 212401 (2011).

[35] A. Wietek and A. M. Läuchli, Sublattice coding algorithm and distributed memory parallelization for large-scale exact diagonalizations of quantum many-body systems, Phys. Rev. E **98**, 033309 (2018).

[36] R. Takashima, H. Ishizuka, and L. Balents, Quantum skyrmions in two-dimensional chiral magnets, Phys. Rev. B **94**, 134415 (2016).

[37] S. Dasgupta, S. Zhang, I. Bah, and O. Tchernyshyov, Quantum Statistics of Vortices from a Dual Theory of the XY Ferromagnet, Phys. Rev. Lett. **124**, 157203 (2020).

[38] H. Ochoa and Y. Tserkovnyak, Quantum skyrmionics, Int. J. Mod. Phys. B **33**, 1930005 (2019).

[39] A. Roldán-Molina, M. J. Santander, A. S. Nunez, and J. Fernández-Rossier, Quantum fluctuations stabilize skyrmion textures, Phys. Rev. B **92**, 245436 (2015).

[40] J. P. Gauyacq and N. Lorente, A model for individual quantal nano-skyrmions, J. Phys.: Condens. Matter **31**, 335001 (2019).

[41] V. Lohani, C. Hickey, J. Masell, and A. Rosch, Quantum Skyrmions in Frustrated Ferromagnets, Phys. Rev. X **9**, 041063 (2019).
[42] V. Yu. Irkhin and M. I. Katsnelson, On the description of the antiferromagnetism without anomalous averages, Z. Phys. B **62**, 201 (1986).
[43] B. Misra and E. C. G. Sudarshan, The Zenos paradox in quantum theory, J. Math. Phys. **18**, 756 (1977).
[44] E. Joos, H. D. Zeh, C. Kiefer, D. J. W. Giulini, J. Kupsch, and I.-O. Stamatescu, *Decoherence and the Appearance of a Classical World in Quantum Theory* (Springer Verlag, Berlin, Heidelberg, 2013).
[45] H. Hafermann, M. I. Katsnelson, and A. I. Lichtenstein, Metal-insulator transition by suppression of spin fluctuations, Europhys. Lett. **85**, 37006 (2009).
[46] H. C. Donker, H. De Raedt, and M. I. Katsnelson, Decoherence wave in magnetic systems and creation of Neel antiferromagnetic state by measurement, Phys. Rev. B **93**, 184426 (2016).
[47] H. C. Donker, H. De Raedt, and M. I. Katsnelson, Antiferromagnetic order without recourse to staggered fields, Phys. Rev. B **98**, 014416 (2018).
[48] H. Abraham *et al.*, QISKIT: An open-source framework for quantum computing (Qiskit community, qiskit.org, 2019).
[49] I. A. Iakovlev, O. M. Sotnikov, and V. V. Mazurenko, Supervised learning approach for recognizing magnetic skyrmion phases, Phys. Rev. B **98**, 174411 (2018).
[50] I. A. Iakovlev, O. M. Sotnikov, and V. V. Mazurenko, Profile approach for recognition of three-dimensional magnetic structures, Phys. Rev. B **99**, 024430 (2019).
[51] See Supplemental Material at http://link.aps.org/supplemental/10.1103/PhysRevB.103.L060404 for additional information on the ED method used in this work, comparison of the classical and quantum ground state energies, the connection between classical and quantum skyrmions, and how to distinguish quantum skyrmions of different types.
[52] B. Berg and M. Lüscher, Definition and statistical distributions of a topological number in the lattice O(3) σ-model, Nucl. Phys. B **190**, 412 (1981).
[53] J. D. Z. Bai, J. Dongarra, A. Ruhe, and H. van der Vorst, *Templates for the Solution of Algebraic Eigenvalue Problems: A Practical Guide* (Society for Industrial and Applied Mathematics, Philadelphia, 2000).
[54] H. D. Rosales, D. C. Cabra, and P. Pujol, Three-sublattice skyrmion crystal in the antiferromagnetic triangular lattice, Phys. Rev. B **92**, 214439 (2015).
[55] Y. Taguchi, Y. Oohara, H. Yoshizawa, N. Nagaosa, and Y. Tokura, Spin chirality, Berry phase, and anomalous Hall effect in a frustrated ferromagnet, Science **291**, 2573 (2001).
[56] N. Kanazawa, Y. Onose, T. Arima, D. Okuyama, K. Ohoyama, S. Wakimoto, K. Kakurai, S. Ishiwata, and Y. Tokura, Large Topological Hall Effect in a Short-Period Helimagnet MnGe, Phys. Rev. Lett. **106**, 156603 (2011).
[57] K. S. Denisov, I. V. Rozhansky, N. S. Averkiev, and E. Lähderanta, A nontrivial crossover in topological Hall effect regimes, Sci. Rep. **7**, 17204 (2017).
[58] R. Shindou and N. Nagaosa, Orbital Ferromagnetism and Anomalous Hall Effect in Antiferromagnets on the Distorted fcc Lattice, Phys. Rev. Lett. **87**, 116801 (2001)
[59] M. Hoffmann, J. Weischenberg, B. Dupé, F. Freimuth, P. Ferriani, Y. Mokrousov, and S. Heinze, Topological orbital magnetization and emergent Hall effect of an atomic-scale spin lattice at a surface, Phys. Rev. B **92**, 020401(R) (2015).
[60] J.-P. Hanke, F. Freimuth, A. K. Nandy, H. Zhang, S. Blügel, and Y. Mokrousov, Role of Berry phase theory for describing orbital magnetism: From magnetic heterostructures to topological orbital ferromagnets, Phys. Rev. B **94**, 121114(R) (2016).
[61] M. dos Santos Dias, J. Bouaziz, M. Bouhassoune, S. Blügel, and S. Lounis, Chirality-driven orbital magnetic moments as a new probe for topological magnetic structures, Nat. Commun. **7**, 13613 (2016).
[62] F. R. Lux, F. Freimuth, S. Blügel, and Y. Mokrousov, Engineering chiral and topological orbital magnetism of domain walls and skyrmions, Commun. Phys. **1**, 60 (2018).
[63] S. Grytsiuk, J.-P. Hanke, M. Hoffmann, J. Bouaziz, O. Gomonay, G. Bihlmayer, S. Lounis, Y. Mokrousov, and S. Blügel, Topological chiral magnetic interactions driven by emergent orbital magnetism, Nat. Commun. **11**, 511 (2020).
[64] A. Kirilyuk and T. Rasing, Magnetization-induced-second-harmonic generation from surfaces and interfaces, J. Opt. Soc. Am. B **22**, 148 (2005).
[65] O. A. Aktsipetrov, T. V. Murzina, E. M. Kim, R. V. Kapra, A. A. Fedyanin, M. Inoue, A. F. Kravets, S. V. Kuznetsova, M. V. Ivanchenko, and V. G. Lifshits, Magnetization-induced second- and third-harmonic generation in magnetic thin films and nanoparticles, J. Opt. Soc. Am. B **22**, 138 (2005).
[66] V. K. Valev, A. V. Silhanek, W. Gillijns, Y. Jeyaram, H. Paddubrouskaya, A. Volodin, C. G. Biris, N. C. Panoiu, B. De Clercq, M. Ameloot, O. A. Aktsipetrov, V. V. Moshchalkov, and T. Verbiest, Plasmons reveal the direction of magnetization in nickel nanostructures, ACS Nano **5**, 91 (2011).
[67] Z. Sun, Y. Yi, T. Song, G. Clark, B. Huang, Y. Shan, S. Wu, D. Huang, C. Gao, Z. Chen, M. McGuire, T. Cao, D. Xiao, W.-T. Liu, W. Yao, X. Xu, and S. Wu, Giant nonreciprocal second-harmonic generation from antiferromagnetic bilayer CrI_3, Nature (London) **572**, 497 (2019).